

Chapter 4

The Discovery of “Ultradense HII Regions”: The Early Stages of Massive Star Cluster Evolution

4.1 Background

In the previous two chapters, super star clusters visible in optical light have been discussed at great length. Some of these clusters are unambiguously young (where I define young to mean < 10 Myr) compared to the age of a typical globular cluster in the Milky Way. However, once these clusters have emerged from their birth cocoons and are visible in optical light, they are well into their adolescence. If massive star cluster formation follows a process similar to that of individual massive star formation, then the earliest stages of clusters evolution will be hidden from optical and UV observations by large amounts of dust and molecular material from which the clusters were formed. Hence, studies of this early phase of cluster evolution require observations at longer wavelengths which are relatively immune to the effects of dust scattering and absorption by the natal material.

If young SSCs are indeed hidden at ultraviolet and optical wavelengths as the result of absorption by surrounding dust, the bulk of their bolometric luminosities should be radiated in the mid- to far-infrared regimes due to the re-processing by dust. With this in mind, it is logical to predict that the youngest SSCs should not be visible at wavelengths shortward of infrared, they should be extremely luminous in the mid- to far-infrared, and they should have radio emission consistent with very dense HII regions.

In this chapter the detection of five such embedded ultra-young clusters discovered in

the radio continuum and confirmed with mid-infrared imaging is presented. The analysis of the radio data was originally in collaboration with H. Kobulnicky, and here I present my own analysis of the radio data and only highlight aspects for which H. Kobulnicky was primarily responsible.

4.2 Observations and Data Reduction

4.2.1 VLA Radio Continuum Observations

Aperture synthesis radio continuum observations were carried out by H. Kobulnicky with the NRAO Very Large Array using a variety of frequencies and array configurations from 1995 through 1996. Observations of 2 cm (15.0 GHz) and 6 cm (4.58 GHz) were obtained with the B and A arrays, respectively, allowing for relatively well matched synthesized beams at the two wavelengths. Lower resolution observations were also made in the C and D arrays which are not discussed here. The uv ¹ coverage for the 2 cm and 6 cm observations produced a clean beam size of $0.''82 \times 0.''40$, highly elongated in the north-south direction due to the southern declination of He 2-10 (declination ≈ -26 degrees). Five radio knots were identified, which are labeled 1-5 from west to east. The uncertainty in the absolute flux calibration is $\sim 5\%$, based on variability of the standard sources used for calibrations (0834-201 and 3C273). For the assumed distance of 9 Mpc, 1 mJy corresponds to a luminosity of 9.2×10^{25} erg s⁻¹ Hz⁻¹ or 9.2×10^{18} W Hz⁻¹. The resulting fluxes are shown in Table 4.1.

4.2.2 Gemini Mid-Infrared Observations

Observations in the mid-infrared were made using the OSCIR imager on the Gemini North telescope during the scheduled OSCIR mini-queue in February 2001. Unfortunately, due to high winds, only a total of 10 minutes of “on source” integration time was possible

¹ Note that here “ uv ” does *not* stand for “ultraviolet”. Because the spatial resolution of observations is dependent on the wavelength and spacing of the radio antennae, radio observations taken with multi-element arrays are only sensitive to discrete spatial scales. The Fourier transform of these spatial scales are commonly mapped onto two orthogonal directions, u and v , and therefore “ uv coverage” refers to how well the range of possible physical scales is sampled by a given set of observations.

Table 4.1: Properties of Individual Radio Knots

Parameter	Knot 1	Knot 2	Knot 3	Knot 4	Knot 5
R.A. (2000)	08 36 15.01	08 36 15.06	08 36 15.13	08 36 15.23	08 36 15.31
Dec. (2000)	-26 24 33.81	-26 24 33.98	-26 24 34.13	-26 24 34.00	26 24 34.61
$S_{2\text{cm}}$ (mJy)	0.94 ± 0.19	1.06 ± 0.21	0.89 ± 0.18	1.73 ± 0.34	1.04 ± 0.21
$S_{6\text{cm}}$ (mJy)	0.82 ± 0.16	0.56 ± 0.11	0.89 ± 0.18	1.10 ± 0.22	0.57 ± 0.12
α_2^6	0.11 ± 0.14	0.53 ± 0.14	0.00 ± 0.14	0.38 ± 0.14	0.51 ± 0.14
$Q_{Lyc} \times 10^{51}$	8.9	10.0	5.4	9.9	6.5
$N_* 07V$	890	1000	540	990	650

using only a single filter. Two sets of 5 minute observations (with small offsets in pointing) were made of He 2-10 using the N-band ($\bar{\lambda} \sim 10.8 \mu\text{m}$) filter. Throughout the observations, standard chopping and nodding techniques were employed in order to subtract the thermal sky background. The FWHM of the standard stars was in the range of $0.''7 - 0.''8$ throughout the observations. The field of view of the Gemini images presented in this paper is $9.''4 \times 9.''4$, and the pixel scale is $0.''089$.

The images were reduced using the OREDUCE task in the GEMINI/OSCIR package available via the Image Reduction and Analysis Facility (IRAF). The data were calibrated using the standard stars α CrB, β Leo, and γ Pix. I adopted the N-band magnitudes given by Tokunaga (1984) for α CrB and β Leo. The N-band magnitude of γ Pix was calculated using the absolutely flux calibrated spectrum given by Cohen et al. (1999) and the OSCIR filter transmission curve. The flux density in mJy was then computed using the zeropoint values found on the OSCIR webpage (ZP= 37.8 Jy). Point spread functions (PSFs) were build using the standard star observations, and photometry was obtained by using psf-fitting in the IRAF task DAOPHOT. The absolute uncertainty in the source fluxes are $\sim 20\%$ and dominated by the uncertainties in the N-band magnitudes of the standard stars ². However, the relative uncertainties in the source fluxes are significantly smaller ($\lesssim 5\%$ for the brightest two sources).

The total N-band flux found from this image is 660 ± 130 mJy. This value is in reason-

² As these fluxes become better characterized, it may be possible to reduce this absolute error in the coming years. At present, mid-infrared standard stars are generally not well characterized.

able agreement with that given by Telesco et al. (1993), who measured the integrated N-band flux of He 2-10 to be 600 ± 40 mJy. Both of these values, however, are substantially smaller than that found by Sauvage et al. (1997) who find an N-band flux of 1.06 Jy. This discrepancy is probably due to three factors: (1) large differences in the N-band filter transmission profiles; (2) an attempt by Sauvage et al. to incorporate a color term in their photometric calibration; and (3) non-photometric conditions during the observations of Sauvage et al. With regard to point (2), the color term correction applied by Sauvage et al. is almost certainly incorrect. They extrapolated their observed $10.1 \mu\text{m}$ flux to the N-band assuming a spectral energy distribution of $f_\nu \propto \nu$; however, the spectral energy distribution of He 2-10 near $10 \mu\text{m}$ is actually decreasing rapidly with frequency. Note also that Sauvage et al. assumed the thermal-IR emission is coincident with the optically visible starburst. As can be seen in Figures 4.1 and 4.2, the thermal-IR emission coincides with the thermal radio emission and is *not* associated with the optically visible SSCs.

Given these issues with the Sauvage et al. N-band flux and the agreement between the value I derive and the value of Telesco et al., I do not believe the discrepancy with this data and the Sauvage et al. data is a concern. Furthermore, if a blackbody spectrum is fit to the IRAS $12 \mu\text{m}$ and $25 \mu\text{m}$ data points and extrapolated to $10.8 \mu\text{m}$, the predicted flux is 640 mJy, in excellent agreement with the observed value presented here.

It is also necessary to point out that the extent to which emission from fine structure nebular lines (e.g., [Ar III] $8.9 \mu\text{m}$, [S IV] $10.5 \mu\text{m}$, and [Ne II] $12.8 \mu\text{m}$) and polycyclic aromatic hydrocarbons (PAHs, at $8.6 \mu\text{m}$, $11.3 \mu\text{m}$, and $12.6 \mu\text{m}$) might be contaminating the observed fluxes in the N-band filter is not known. Starburst galaxies are known to exhibit a wide range of strengths for these features (Madden 2000). A recent mid-IR spectrum of the dwarf starburst galaxy NGC 5253 presented by Crowther et al. (1999) shows virtually no sign of PAH emission (this is the only other galaxy known to host similar radio sources which has been studied in the mid-IR to date). Therefore, I tentatively assume that these features do not contribute substantially to the N-band flux, but follow-up mid-IR spectroscopy is planned to investigate this

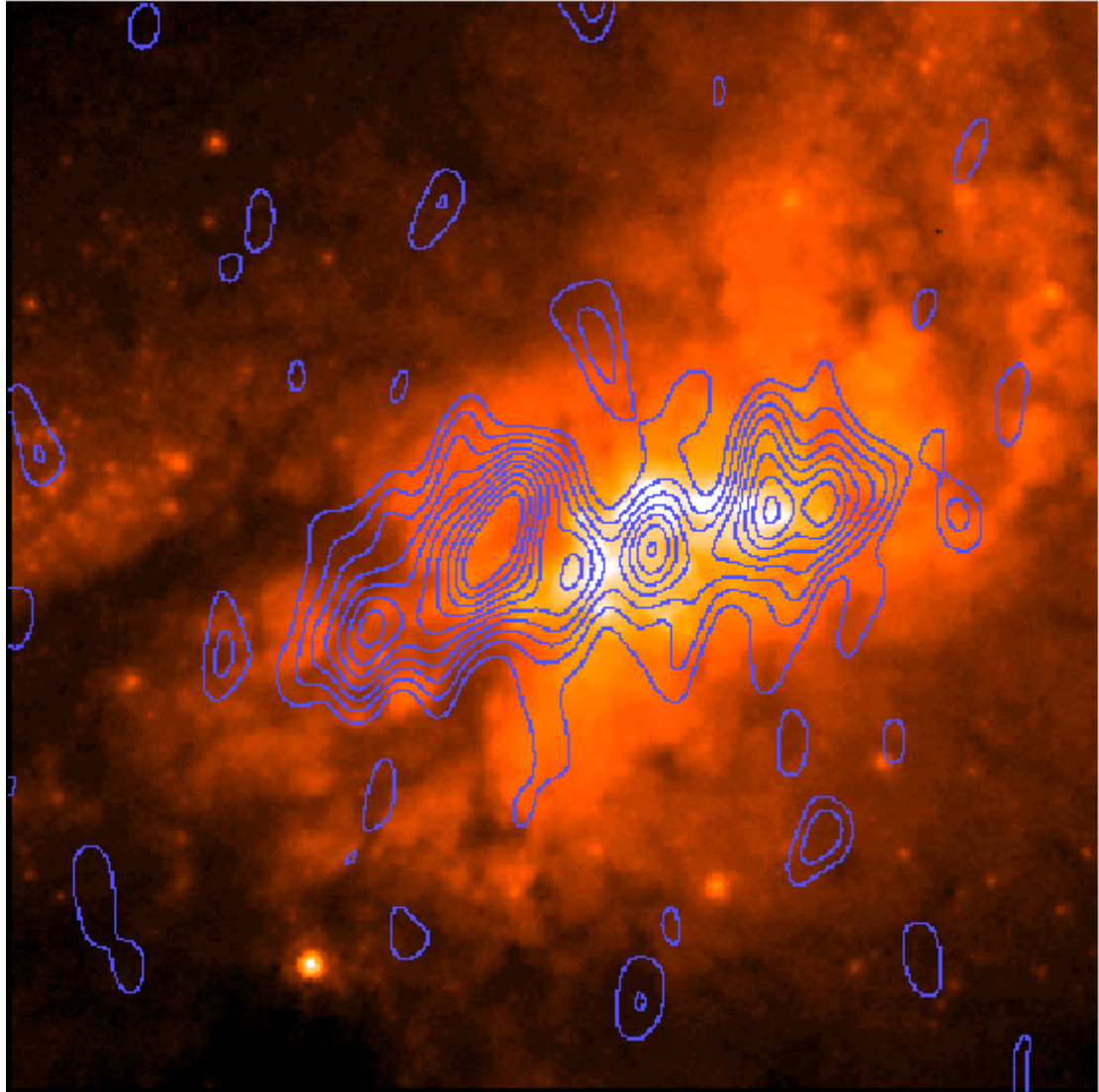


Figure 4.1: HST WFPC2 F555W (V-band) image of He 2-10 in colorscale overlaid with VLA B-array 2 cm radio continuum contours with a synthesized beam of $0.''82 \times 0.''40$ FWHM. This image is approximately $9.''4 \times 9.''4$, and shown at the same scale and orientation as Figure 4.2. It is clear that the 2 cm radio sources do not correspond to the optical SSCs.

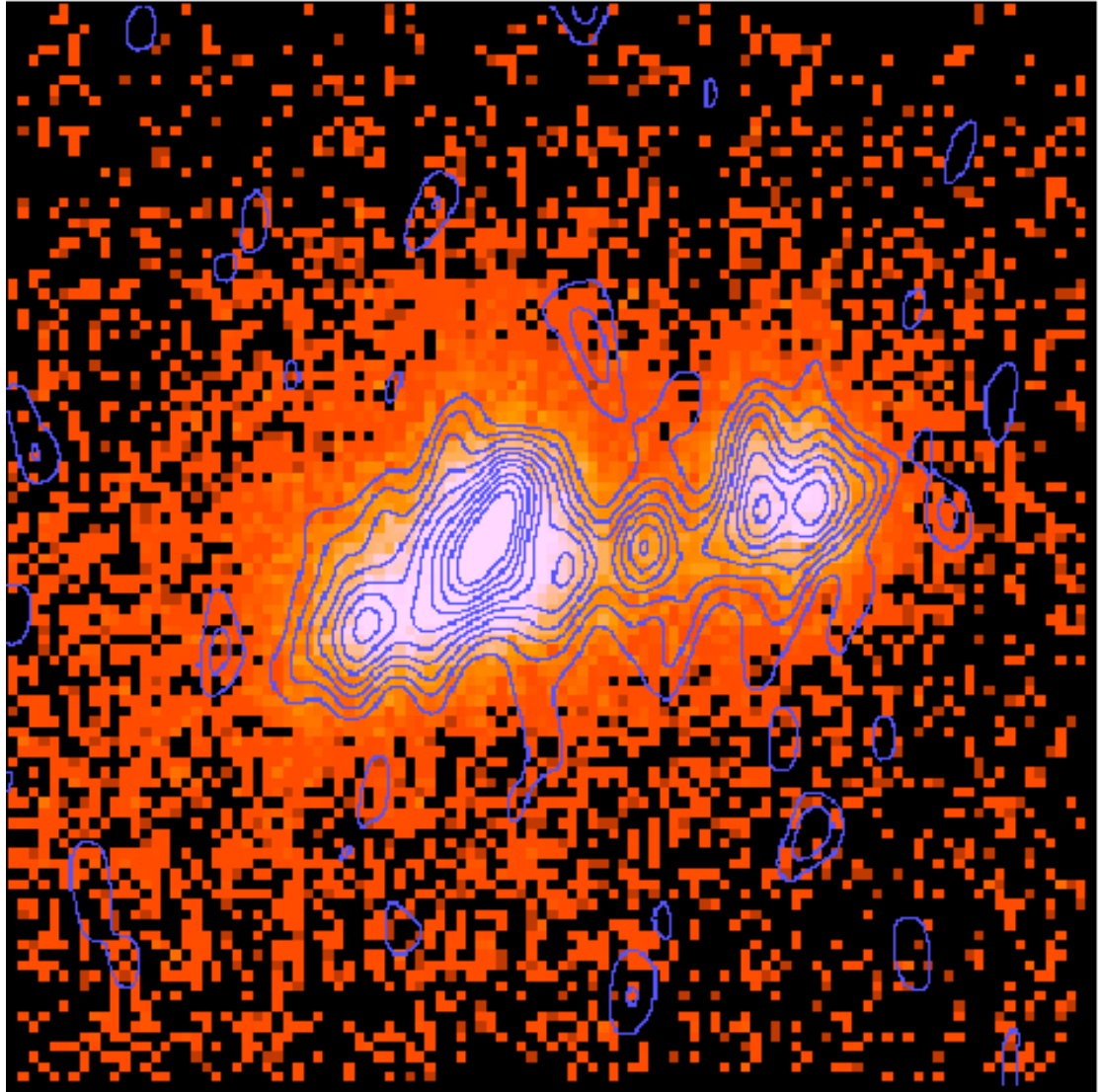


Figure 4.2: Gemini N-band image of He 2-10 in colorscale overlaid with the same 2 cm contours as Figure 4.1. At least three of the five radio sources are also strong mid-IR sources. The mid-IR morphology is strongly correlated to the radio morphology, but quite dissimilar from the optical morphology.

possibility.

The combined N-band flux of the three “detected” radio sources compared with the total N-band flux of He 2-10 (as derived in this chapter, quoted in Telesco et al. 1993, or estimated from the IRAS flux) suggests that at least $\sim 60\%$ of the $10.8 \mu\text{m}$ flux of the *entire* galaxy can be attributed to only these three objects. Based on the relative morphologies of the diffuse N-band flux seen in the Gemini image, it appears that very little of the remaining flux is due to dust heated by the starburst component seen in the UV and optical bands. Most of the diffuse background has a morphology similar to that of the radio sources, but on a larger scale. Therefore, it is possible that some of this diffuse background flux in the N-band arises from dust which is heated by radiation escaping from the embedded H II regions. If this is indeed the case, then nearly all of the observed N-band flux, and by extension nearly all of the observed flux from He 2-10 in the IRAS bands would be attributable to these enshrouded stellar clusters. Given the vigorous recent star formation throughout He 2-10, as discussed in Chapter 3, this result is rather remarkable.

4.3 Comparison of Optical, Radio, and Mid-IR Images

Figures 4.1 and 4.2 show the 2 cm radio contours overlaid on both the optical V-band HST image (from Chapter 3) and the Gemini N-band image. The morphology of the radio emission and the mid-IR emission are nearly identical. However, these images reveal a striking *dissimilarity* between the optical morphology and that of the radio and mid-IR. Five radio knots are apparent (labeled knots 1 through 5 from west to east), three (possibly four) of which are also extremely bright N-band sources — knots #1, 4, and 5 are readily detected and #2 is likely to be blended with #1 (the remaining radio source may also have mid-IR emission not detected in the signal to noise allowed for in only the 10 minutes of integration time achieved).

The absolute coordinates of the radio map are accurate to $0.''05$, while the HST image are uncertain by $\sim 0.''5$, limited by the positional uncertainties of the guide stars from the Guide Star Catalog (Lasker et al. 1990). This leads to a relative positional uncertainty between the

radio and optical image of $\sim 0.''5$. Although there is a relative uncertainty of $0.''5$ between the radio and optical image, there is no obvious correlation between the morphology 6-8 optical/UV star clusters in the nuclear region of He 2-10 (distributed in a chevron configuration) and the radio point sources. Given any possible $0.''5$ translation of the optical image, no more than 2 of the radio sources would have a corresponding optical counterpart. Given the high extinction in the core of this galaxy, it is not surprising that the optical and radio morphologies are so different.

4.4 The Nature of These Radio Sources

In order to determine the nature of these radio sources, let us first review the observational constraints which must be satisfied. (1) There appear to be at least five such sources in He 2-10 at sufficient signal to noise to be detected with these radio observations. (2) Each of these sources has a *positive* spectral index ($\alpha > 0$, where $S_\nu \propto \nu^\alpha$: higher fluxes at shorter wavelengths). (3) The sources have 2 cm and 6 cm luminosities of $\sim (5 - 10) \times 10^{25} \text{ erg s}^{-1} \text{ Hz}^{-1}$. (4) Based on a comparison with lower quality data from 1984 and 1985, these same radio sources are present with the same fluxes (within the relative error) over roughly ten years. (5) These radio sources each have corresponding $10 \mu\text{m}$ fluxes of $\sim 100 \text{ mJy}$ at 9 Mpc. With these constraints in mind, possible types of radio sources can be put to the test.

4.4.1 Could These Objects be Supernovae Remnants?

Some of the most “conventional” radio objects are supernovae (SNe) and supernovae remnants (SNR). He 2-10 has recently undergone a great deal of star formation (Chapter 3), therefore it would be quite surprising if this galaxy were not prodigiously producing SNe. This expected multiplicity easily passes criterion (1).

The first clue that these objects are not SNR is their positive spectral index; typical SNR have $\alpha < -0.4$, although not all SNR obey this “rule” — in particular, there is a class of “composite” or “plerionic” SNR (as coined by Weiler & Panagia 1978) that are known to have

atypically flat spectral indices ($-0.3 < \alpha < 0.0$). In fact, in the first few hundred days after an SNe explosion, α can actually be positive (Weiler et al. 1986). Consequently, the positive spectral indices of the radio objects in He 2-10 make it extremely unlikely that they could be SNR, failing criterion (2). Since the radio fluxes of SNe have typical decay times of a few years (Weiler et al. 1986), criterion (4) is almost certainly failed.

Criterion (5) is also failed by SNR. In the survey of Arendt (1989), he found that only $\sim 1/3$ of SNR in the galaxy are even visible in the IRAS observations. The SNR which are apparent in the IRAS observations have $12 \mu\text{m}$ fluxes which are almost exclusively less than 10^3 Jy at galactic distances of ~ 10 kpc. At the distance of He 2-10, these SNR would have $10 \mu\text{m}$ fluxes $\lesssim 1$ mJy (two orders of magnitude fainter than the $10 \mu\text{m}$ fluxes observed for the objects in He 2-10).

Finally, is it possible that these objects could be old SNR which are fading at a slower rate than bright young SNR? The luminosities of typical SNR in the Milky Way are several orders of magnitude less luminous, ranging from $8 \times 10^{21} \text{ erg s}^{-1} \text{ Hz}^{-1}$ for 1000 yr old remnants to $7 \times 10^{24} \text{ erg s}^{-1} \text{ Hz}^{-1}$ for Cas A (330 yr old remnant). At the distance of He 2-10, a bright young SNR like Cas A would be only a $\sim 2\sigma$ detection in these observations, thus failing criterion (3). In this case, 4 out of 5 observational criteria were failed, and SNR are ruled out as a plausible origin for the radio objects in He 2-10.

4.4.2 Could These Objects be AGN?

Active galactic nuclei (AGN), such as radio loud quasars, can be quite luminous radio sources. From the sample of Kellermann et al. (1989), such quasars can be brighter than ~ 10 mJy at 6 cm, easily passing criterion (3). Some AGN are also known to have flat to slightly positive spectral indices ($\alpha \gtrsim -0.3$, e.g., Nagar et al. 2000, although some of these “AGN” are not conclusively ruled out as star forming nuclei). Therefore, criterion (2) is not necessarily failed in this case. It is also not possible to rule out AGN based on criterion (4); while AGN are known to have variations in their radio luminosities, these variations are not necessarily mono-

tonic. An AGN could very plausibly be observed at roughly the same luminosity in observations separated by 10 years. The mid-infrared luminosities of AGN (dominated by the reprocess of radiation in their dust tori) could also easily surpass criterion (5) (Urry & Padovani 1995).

Criterion (1) presents the real hurdle for AGN as candidates for the radio objects in He 2-10. While in some galaxy mergers involving large spiral galaxies which each hosted its own AGN, the young merger remnants may still have two discrete nuclei and therefore may also contain two AGN. However, even a single AGN is unlikely to be found in a dwarf galaxy, and five AGN in a single dwarf galaxy even more unlikely. As a result AGN are ruled out as a possibility for the radio sources in He 2-10.

4.4.3 Could These Objects be Enshrouded H II Regions?

Compact H II regions are strong sources of free-free emission and represent most plausible option for the origin of the radio sources in He 2-10. From Chapters 2 and 3, it is clear that massive star clusters are formed in starburst galaxies such as He 2-10. If the star formation in He 2-10 has been roughly continuous over the last 10 Myr, then for ~ 80 SSCs formed in this time period, we should expect ~ 8 SSCs to be formed every million years. Therefore, it is entirely plausible that several radio sources attributable to SSC formation should be present, and criterion (1) is easily passed.

Flat or positive spectral indices like the ones observed in He 2-10 are common for compact H II regions in the Galaxy on sub parsec scales (e.g, see the compilation of Wood & Churchwell 1989a for ultra-compact H II regions, UCH IIs). This type of spectral energy distribution is well understood in the case of UCH IIs as thermal bremsstrahlung emission which has a high turnover frequency due to extremely high electron densities, thereby meeting criterion (2).

Criterion (3) could not be met by individual massive stars embedded in dense H II regions, as is the case for UCH IIs, but rather would require several hundred massive stars to create such luminous H II regions at radio wavelengths. However, this is exactly what one should expect to observe when massive star clusters, such as SSCs, are early in their evolution.

Criterion (5) can also be met in this way; individual UCH II regions in the Galaxy have typical $10 \mu\text{m}$ fluxes of 10^{2-3} Jy (Wood & Churchwell 1989b), which is not sufficient to match the observed $10 \mu\text{m}$ fluxes. However, several hundred to a thousand UCH II regions (which we might expect to find in extremely young clusters) would easily meet this requirement.

Finally, we come to criterion (4); ten years is an extremely short timescale in terms of SSC evolution, and any measurable change in the observed flux over this timescale is not expected (e.g., Leitherer et al. 1999). I will discuss the timescale on which we might expect to find such dense embedded H II regions in §4.6.1.

The most plausible conclusion is that the radio sources in He 2-10 are extremely dense H II regions powered by massive star clusters (SSCs) early in their evolution. In fact, perhaps we should even *expect* to find such objects in starburst galaxies.

4.5 Physical Properties of the Dense H II Regions

Given the luminosities and radio spectral energy distributions of H II regions, their physical parameters such as emission measure, size, and electron density can be estimated. In Figure 4.3 the 2 cm (14.9 GHz) and 6 cm (4.8 GHz) fluxes of each point source are plotted to show the rising nature of the radio spectrum toward higher frequencies. Since the absorption coefficient for optically thick free-free absorption, κ_ν , is proportional to ν^{-2} , there is a turnover frequency ν_t below which a plasma becomes optically thick to radiowave frequencies and the spectral index changes from $\alpha = -0.1$ to positive values, approaching the blackbody limit of $\alpha = 2$ as $\tau \rightarrow \infty$.

The spectral energy distribution for each of the three objects detected with Gemini are shown in Figure 4.4. In these plots, the radio and mid-IR data points are combined with the estimated IRAS fluxes for each knot. Since the IRAS observations are not at a sufficient spatial resolution to isolate the individual sources, these fluxes were derived for each knot by multiplying the total IRAS fluxes for He 2-10 by the fractional contribution of each knot to the total N-band flux (in other words, it was assumed that the fraction of light each source contributed to

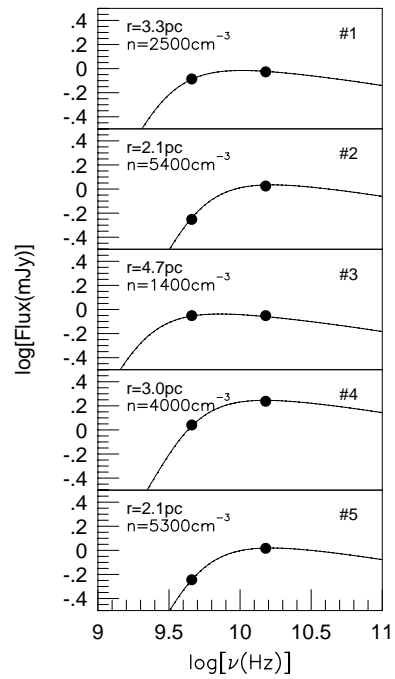


Figure 4.3: VLA 6 cm and 2 cm fluxes for the five radio knots in He 2-10. Model spectral energy distributions are shown for an ionized sphere of hydrogen with uniform temperature and density. The radius and density used to model each source are listed in the upper left corner.

the N-band will be the same relative fraction in the IRAS observations). These spectral energy distributions bear a remarkable resemblance to those for ultracompact H II regions (e.g., Wood & Churchwell 1989b).

4.5.1 Emission Measures

Using the analytical approximation of Mezger & Henderson (1967), the emission measure, $EM = \int n_e^2 dl$, can be estimated given an electron temperature, T , the observing frequency, ν , and the optical depth at that frequency, τ .

$$EM (\text{cm}^{-6} \text{ pc}) = 12.2 \left[\frac{T_e}{(\text{K})} \right]^{1.35} \left[\frac{\nu}{(\text{GHz})} \right]^{2.1} \tau. \quad (4.1)$$

The positive spectral index for these sources arises from free-free emission where $\tau \gtrsim 1$, therefore I assume $\tau = 1$ as a lower limit. Adopting $T_e=6000$ K based on the spectroscopy of Kobulnicky et al. (1999), the resulting emission measures are in excess of $\sim 5 \times 10^7 \text{ cm}^6 \text{ pc}$ at 6 cm (for $\tau > 1$ these emission measures will be correspondingly higher).

4.5.2 Comparison With Model H II Regions

In order to better constrain the properties of these sources, I have created model H II regions (spherical, uniform electron density and electron temperature) of radius, R , electron temperature, T_e , and electron density, n_e . Only free-free emission and absorption processes are considered, and a temperature of 6000 K is assumed, based on the work of Kobulnicky et al. (1999). The models are somewhat insensitive to variation in temperature in a reasonable range about this value; since the optical depth goes as $\tau \propto T^{-3/2}$, the main effect of changing the assumed temperature is to shift the turnover frequency. For a reasonable range in temperatures (e.g., 5000 - 8000 K), the turnover frequency could only shift by $\lesssim 0.5$ GHz.

In Figure 4.3 the resulting spectral energy distributions are shown for a range of models. The luminosities and spectral indices of these compact sources are well-fit by model H II regions with a radius of 2—5 pc, and electron densities of 1400-5400 cm^{-3} at a distance of 9 Mpc. In

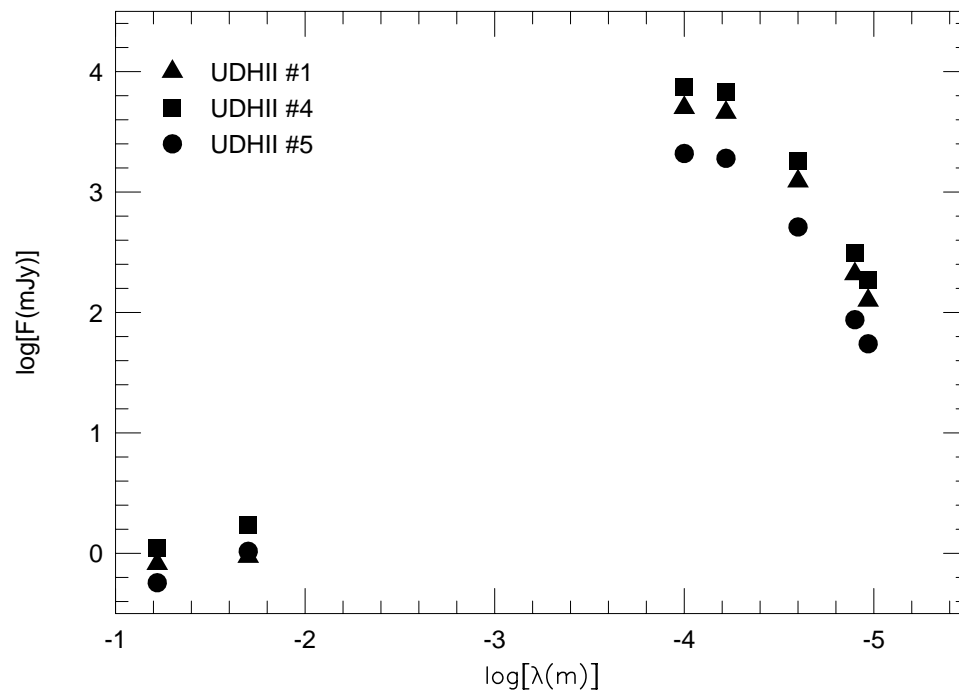


Figure 4.4: The spectral energy distribution of the UDHIIs in He 2-10. The $12 \mu\text{m}$, $25 \mu\text{m}$, $60 \mu\text{m}$, and $100 \mu\text{m}$ have been estimated by multiplying the total IRAS flux of He 2-10 by the fractional percentage of the total N-band flux for each UDHI I.

reality, we might expect that the radio structures are not single monolithic H II regions, but a collection of smaller H II regions with higher densities embedded in a lower density medium, however this picture is not yet clear.

4.5.3 Limits on the Contribution From SNe

In § 4.4 it was clear that these radio sources could not be SNe or SNR, but rather are most likely to be embedded H II regions. Never the less, it is possible that non-thermal flux from SNe and SNR might be contributing to the observed fluxes. The lowest frequency observed (in this case 4.58 GHz) can be used to place an *upper* limit on both the SN frequency and the fraction of the highest frequency flux (in this case 15 GHz) which might be due to non-thermal emission. In order to make these estimates, it is necessary to examine the case, as an *upper* limit, that all of the 4.8 GHz flux is due to synchrotron radiation. The maximum amount of non-thermal emission at 15 GHz is given by,

$$S_{15 \text{ GHz}} \leq \left(\frac{15 \text{ GHz}}{4.58 \text{ GHz}} \right)^\alpha S_{4.58 \text{ GHz}}. \quad (4.2)$$

Adopting $\alpha \sim -0.8$ (typical of synchrotron sources in the Galaxy, Condon 1992), the maximum amount of non-thermal flux which could be contaminating the 15 GHz observations is $\lesssim 0.4 S_{4.58 \text{ GHz}}$.

Following Condon & Yin (1990) and Condon (1992), the SN frequency can also be constrained. The relation between the SN frequency and non-thermal luminosity is given by,

$$\frac{L_{\text{non-thermal}}}{10^{22} \text{ W Hz}^{-1}} \approx 13 \left(\frac{\nu}{\text{GHz}} \right)^\alpha \left(\frac{\nu_{\text{SN}}}{\text{yr}^{-1}} \right). \quad (4.3)$$

As an example using knot 4 (the brightest knot in this sample), and again adopting $\alpha \sim -0.8$ (Condon 1992), the maximal SN frequency is given by $\nu_{\text{SN}} \lesssim 2 \times 10^{-4} \text{ yr}^{-1}$. Using the Starburst99 models of Leitherer et al. (1999), this SN frequency is almost an order of magnitude less than the SN frequency expected when SN begin to occur at an age of $\sim 4 \text{ Myr}$ for a model cluster. Therefore, it is unlikely that SNe have begun to occur in significant numbers, if at

all, and we expect the non-thermal contamination in these data to be insignificant. Moreover, the paucity of SNe puts an absolute upper limit on the ages of these clusters of ~ 4 Myr (although, as we will see in § 4.6.1 the ages can be constrained to much younger values with other methods).

4.5.4 Ionizing Radiation

The production rate of Lyman continuum photons, and thus the stellar content of each of the embedded H II regions can be estimated from the thermal radio luminosity following Condon (1992),

$$Q_{Ly\alpha} \geq 6.3 \times 10^{52} \text{ s}^{-1} \left(\frac{T_e}{10^4 \text{ K}} \right)^{-0.45} \left(\frac{\nu}{\text{GHz}} \right)^{0.1} \left(\frac{L_{thermal}}{10^{27} \text{ erg s}^{-1} \text{ Hz}^{-1}} \right). \quad (4.4)$$

Since the non-thermal component becomes weaker at higher frequencies, the luminosity measured at the highest radio frequency (in this case 15 GHz) is used to determine $Q_{Ly\alpha}$. The resulting values determined from this method are presented in Table 4.1.

One should also bear in mind that the $Q_{Ly\alpha}$ values determined with this method could suffer from two different problems: (1) if the source is, in fact, optically thick even at the highest frequency measured, this method will *underestimate* the actual ionizing luminosity, and (2) if there is contamination from non-thermal emission in the beam at the frequency used, the ionizing luminosity will be *overestimated*. However, the overall non-thermal background of the galaxy will tend to be resolved out with the small synthesized beams used in these observations. Therefore the only non-thermal flux which might boost the 15 GHz luminosity would be SNe within the objects themselves. I estimate the maximum affect this might have in § 4.5.3, and do not expect any significant contribution.

Further evidence for deriving the ionizing luminosity from this method comes by comparing the total $Q_{Ly\alpha}$ calculated for He 2-10 using the 15 GHz flux with the total $Q_{Ly\alpha}$ calculated from optical H α observations; $Q_{Ly\alpha}$ determined in the radio should include the ionizing flux apparent in optical light, the ionizing flux which is optically obscured, and any non-thermal

contamination. As a result, if there is non-thermal contamination, the radio $Q_{Ly\alpha}$ cannot be less than the optically determined $Q_{Ly\alpha}$. Conversely, if the radio $Q_{Ly\alpha}$ is less than the optically determined $Q_{Ly\alpha}$ that implies that the radio value is *underestimating* the ionizing luminosity. Kobulnicky & Johnson (1999) find $Q_{Ly\alpha} = 2.0 \times 10^{53} \text{ s}^{-1}$ for the entire galaxy using the 15 GHz luminosity. The Méndez et al. (1999) $H\alpha$ measurement yields $Q_{Ly\alpha} = 2.1 \times 10^{53} \text{ s}^{-1}$, which is only marginally larger than the value determined in the radio. Therefore, I conclude that non-thermal contamination is *not* significantly contributing to the 15 GHz flux, and this method for deriving $Q_{Ly\alpha}$ will not be an overestimation, but rather is quite possibly an underestimation.

4.5.5 Stellar Content

The production rate of Lyman continuum photons from these sources can be used to estimate the number of massive stars powering the observed emission. Following the convention of Vacca (1994) and Vacca et al. (1996), a “typical” O-star (type O7V) produces $Q_{Ly\alpha} = 1.0 \times 10^{49} \text{ s}^{-1}$. Using this method, 20,000 such O stars are required to power the total observed radio ionizing luminosity from He 2-10. Each of the individual embedded clusters require between 500 and 1000 equivalent O7V stars in order to produce their ionizing luminosities (see Table 4.1). Thus, each embedded cluster contains more O stars than are found in the entire 30-Doradus nebula in the LMC (~ 200 , Vacca et al. 1995). Using the Starburst99 models of Leitherer et al. (1999) with solar metallicity, Salpeter IMF, an upper mass cutoff of $100 M_{\odot}$, and a lower mass cutoff of $1 M_{\odot}$, starburst knots producing this range of Lyman continuum photons at an age of 1 Myr would have masses of $0.8 - 1.6 \times 10^5 M_{\odot}$ (if the lower mass cutoff is $< 1 M_{\odot}$, these mass estimates will be correspondingly higher). These masses are consistent with those found for the optical SSCs in He 2-10 (Chapter 3) which have already emerged from their birth material, thus strengthening the connection between UDH IIs and SSCs.

Since the star-forming regions seen in these radio observations are not seen even faintly on the HST V- or I-band images (or even in the near-infrared, Vacca et al. in preparation), their

visual extinctions must be quite large. Such large extinction values are consistent with the column density of molecular gas observed in this region (Kobulnicky et al. 1995) and the extinction estimates from the infrared silicate features ($A_V \simeq 30$, Phillips et al. 1984). Given that He 2-10 was already known to contain 31,000 O stars (Conti & Vacca 1994) the additional ~ 4000 O stars contained in these five dense, heavily obscured H II regions represent a significant fraction of the massive stars in He 2-10.

4.6 Discussion

The major result of this chapter is the discovery of multiple optically thick free-free sources, most plausibly dense H II regions powered by extremely young embedded massive star clusters. The majority of these sources do not coincide with features visible in the optical HST images, leading to the conclusion that they are heavily obscured by dust. The combination of high obscuration and high density inferred from the free-free optical depth is consistent with very dense H II regions. While such dense, optically-thick, inverted-spectrum H II regions exist in abundance around *individual* stars in the Galaxy (i.e., ultracompact H II regions; Wood & Churchwell 1989b) this phenomenon had not been previously seen on such large spatial and energetic scales. Because of their similar densities to ultracompact H II regions in the Galaxy, we might term them “ultra dense H II regions” (UDH IIs).

4.6.1 On the Lifetimes of UDH IIs

If UDH IIs are similar to (albeit vastly scaled up) from UCH IIs, it seems likely that the fraction of time a super star cluster spends in the UDH II phase is a small fraction of the massive star lifetime. In accord with the estimated lifetimes of individual UCH II regions based on the number of UCH II regions compared with the number of optically visible O stars in the Galaxy (e.g., Wood & Churchwell 1989a) is $\approx 10 - 15\%$. Indeed, UCH II region lifetimes have been a topic of much discussion since Wood & Churchwell (1989b) introduced the “lifetime problem”; in short, if UCH II regions are significantly overpressured with respect to the surrounding ISM,

they should expand and dissipate on time scales $\approx 10^4$ years. However, the number of UCH II regions observed is greater than is allowed for by this time scale.

Several mechanisms have been proposed to address this issue, most of which are also likely to be applicable to UDH IIs. Wood & Churchwell (1989b) proposed that infalling matter or bow shocks might act to increase the external pressure, thus extending the UCH II phase. It is also possible that the ambient pressure is typically significantly higher than the value used by Wood & Churchwell (1989b), as proposed by de Pree et al. (1995). The lifetimes of UCH II regions could also be extended if they are replenished by material photoevaporated from the surrounding circumstellar disks (e.g., Hollenbach et al. 1994).

The first argument for the extreme youth of UDH II regions is simply by analogy to UCH II regions in the Galaxy. If UDH IIs are composed of individual UCH II regions, we should expect them to have similar lifetimes provided that star formation is relatively instantaneous over the massive star cluster. As is the case for UCH II regions, the densities in UDH IIs are likely to be extremely high, and the implied pressures constitute an over-pressure compared to typical ISM pressures. If the surrounding ISM has typical densities of $n_e \sim 100 \text{ cm}^{-3}$, then these embedded H II regions with densities of $n_e \sim 5000 \text{ cm}^{-3}$ are at an overpressure of ~ 50 . To first order, such over-pressed regions must rapidly expand and disperse on time scales comparable to the sound-crossing time scale which is a few $\times 10^5$ years for $c_s \approx 10 \text{ km s}^{-1}$. However, as discussed above for UCH II regions, it is entirely possible that the ambient pressure around UDH IIs is not “typical” of the global ISM and might present a mechanism for extending the lifetime of the UDH II phase.

The second method to estimate the lifetimes of UDH IIs is to compare the fraction of ionizing stars in UDH II regions with the total number of ionizing stars in the galaxy. The total Lyman continuum photon production rate, Q_{Lyc} , of the UDH II regions in He 2-10 is $4.7 \times 10^{52} \text{ s}^{-1}$ (provided there is no leakage from the enshrouding cocoon that would likely result in associated H α emission). The Q_{Lyc} determined optically for the entire galaxy He 2-10 is $2.1 \times 10^{53} \text{ s}^{-1}$ (Méndez et al. 1999), implying a total $Q_{Lyc} \sim 2.5 \times 10^{53} \text{ s}^{-1}$. Thus, the UDH II

regions contain $0.18\times$ the total ionizing photons. It then follows that if the star formation has been reasonably continuous in this system over the last 10 Myr, a plausible estimate for the typical duration of the UDH II phase is $\sim 18\%$ times the typical massive star lifetime ($\times 10^7$ yr), remarkably in accord with the estimates for individual UCH II regions. This method implies a mean lifetime of roughly 1 – 2 Myr for UDH II regions, although if strong star formation has been occurring over less than 10 Myr, this estimate will be correspondingly lower. A similar method to estimate the lifetimes of UDH IIs is simply to compare the number of clusters which are no longer enshrouded (~ 76 from Chapter 3) to the number of UDH IIs. Given that the optical clusters in He 2-10 are typically less than 10 Myr old, this method implies the UDH II phase only lasts a few $\times 10^5$ years, which is slightly lower than the lifetimes estimated with the first method. While these estimates are very crude, a reasonable lifetime for the UDH II phase is perhaps $\lesssim 1$ Myr.

Perhaps the weakest argument in favor of the extreme youth of UDH II regions comes from their high visual extinctions. In §4.3 it is clear that the UDH II regions are not visible at optical wavelengths. This picture is consistent with UDH IIs being extremely young H II regions still hidden from view by the dust associated with their natal molecular clouds. However, one must also bear in mind that we cannot rule out screens of dust not physically associated with the regions of optically thick free-free emission.

4.6.2 UDH IIs in Other Starburst Systems?

It would be quite surprising if the UDH II phenomenon was unique to He 2-10. If UDH IIs do indeed represent the early stages of SSCs evolution, then they ought to be present in most (if not all) starburst galaxies. High resolution 2 cm and 6 cm radio observations of a large sample of starburst systems acquired in scaled B and A-array configurations with the VLA will be required to examine this issue. To date, such high spatial resolution data generally exist only for more luminous systems like quasars and AGN. In some cases (as will be discussed in the following chapter) perhaps other star-forming galaxies contain dense, heavily obscured H II

regions like the five in He 2-10, but they have simply not been identified as such. Never the less, very little data currently exists which can adequately address the ubiquity of UDH IIs, and this area of research will benefit from an extensive observing campaign.

Turner et al. (2000) detected one such object in the nucleus of the galaxy NGC 5253. NGC 5253 is a dwarf starburst galaxy in the Centaurus group of galaxies at a distance of ~ 4.1 Mpc (Sandage et al. 1994). The radio object in NGC 5253 has estimated properties which are fully consistent with it being a genuine UDH II. In fact, follow-up work by Gorjian et al. (2001) has also confirmed this UDH II with mid-IR Keck observations. Turner et al. estimate that this object has a radius of ~ 2 pc, and has an ionizing photon rate of $Q_{Ly\alpha} \sim 10^{51-52} \text{ s}^{-1}$, in close agreement with the results of this chapter. My own analysis of this system, using the 2 cm fluxes from Turner et al. (1998) and the 1.3 cm fluxes from Turner et al. (2000), indicate a best-fit radius of 3.6 pc and an electron density of $n_e \approx 5000 \text{ cm}^{-3}$ (Figure 4.5) for an electron temperature of 11,000 K (as derived by Kobulnicky et al. 1997). These values are remarkably close to the electron densities and radii found for the UDH IIs in He 2-10 in § 4.5.2.

Arguably the most well known starburst in the local universe is M 82, making it an obvious object for comparison. With a distance of only ~ 3.6 Mpc (Freedman et al. 1994), it can be studied at higher spatial resolution than He 2-10. Radio continuum maps presented in Allen & Kronberg (1998) show 26 compact sources with linear diameters of 3.5 pc ($0.''2$) and 2 cm spectral luminosities of $2.9 \times 10^{24} \text{ erg s}^{-1} \text{ Hz}^{-1}$ to $7.3 \times 10^{25} \text{ erg s}^{-1} \text{ Hz}^{-1}$ (fluxes of 0.2 mJy to 5 mJy). Of the 26 sources in M 82, 22 show distinctly non-thermal spectral indices and are consistent with supernova remnants. Their radio spectra often show turnovers, but only at low frequencies ($\nu < 1$ GHz), due to free-free absorption in the surrounding ionized gas. Only one source has a thermal spectrum typical of an H II region, but it is quite flat with no indication of a turnover due to free-free absorption. de Grijs et al. (2001) suggest that M 82 has possibly undergone several starburst episodes and hosts sites of “fossil” starbursts. Perhaps M 82 is between starburst events, or even possibly post-starburst, and therefore not producing UDH IIs in large numbers.

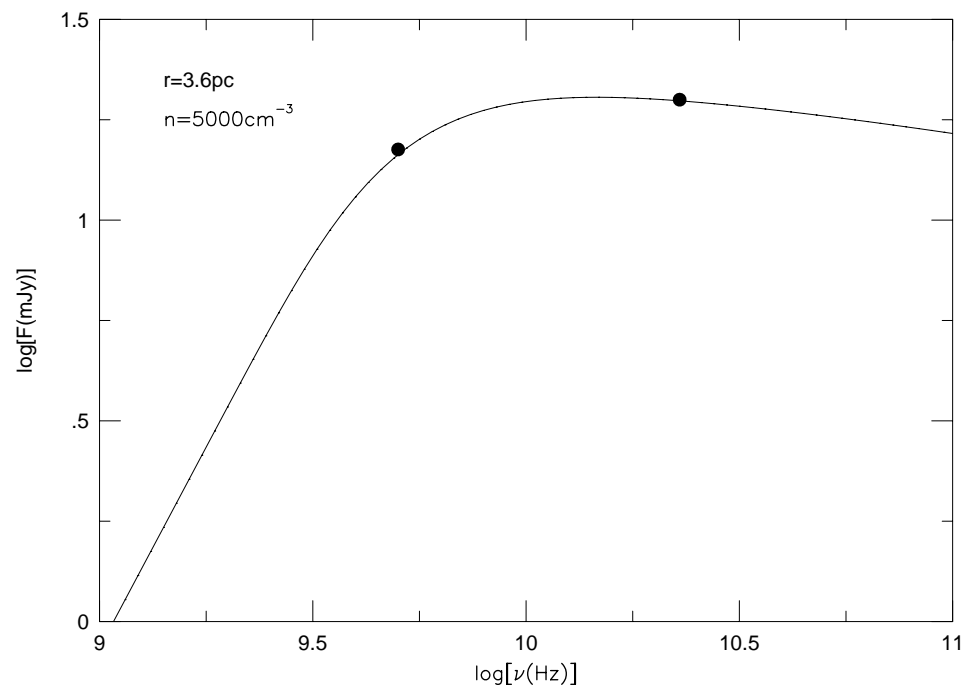


Figure 4.5: Best fit electron density and radius for the UDH II in NGC 5253 detected by Turner et al. (2000). The models are the same as described in § 4.5.2 and use an electron temperature of 11,000 K as derived by Kobulnicky et al. (1997).

4.6.3 Implications for the Infrared-Radio Correlation?

There is a well-known correlation between the infrared and radio fluxes of galaxies over a wide range of Hubble types as first reported by van der Kruit (1971). This relation is typically represented by the logarithmic far-infrared(FIR)-to-radio flux ratio

$$q \equiv \log [(F_{\text{FIR}} / 3.75 \times 10^{12} \text{ Hz}) / S_{1.49\text{GHz}}], \quad (4.5)$$

where F_{FIR} is an approximation of the flux between ~ 40 and $\sim 120 \mu\text{m}$ as

$$F_{\text{FIR}} (\text{W m}^{-2}) \equiv 1.26 \times 10^{-14} (2.58 S_{60\mu\text{m}} + S_{100\mu\text{m}}), \quad (4.6)$$

where $S_{1.49\text{GHz}}$, $S_{60\mu\text{m}}$, and $S_{100\mu\text{m}}$ are the flux densities (in units of $\text{W m}^2 \text{ Hz}^{-1}$) at 1.49 GHz, $60\mu\text{m}$, and $100\mu\text{m}$, respectively.

Over a range of spiral, irregular, and starburst galaxies (see Sanders & Mirabel 1996, and references therein), q is very robust with a small standard deviation; $\langle q \rangle = 2.35 \pm 0.2$.³ For starbursts selected from the IRAS Bright Galaxy Survey, Condon et al. (1991b) find an average value of $q = 2.34 \pm 0.19$. They also find q tends to be higher for the more infrared luminous galaxies. Furthermore, *these galaxies with high q values also tend to have compact radio sources*. Condon et al. hypothesize that this class of ultraluminous infrared galaxies (ULIGs) are powered by dense, compact starbursts which are optically thick at 1.49 GHz, and whose radio flux density is therefore suppressed relative to the FIR. Correcting for the optical depth at 1.49 GHz yields a tighter FIR-radio correlation.

In the extreme case that a galaxy were entirely in the UCH II/UDH II phase, what would its q value be? To answer this question, let us use W49A as an analogy. W49A is one of the most well-studied UCH II complexes in the Galaxy and has been resolved into at least 30 UCH IIs (de Pree et al. 1997). From the Ward-Thompson & Robson (1990) values for $S_{60\mu\text{m}}$ and $S_{100\mu\text{m}}$, $F_{\text{FIR}} = 2.6 \times 10^{-9} \text{ W m}^{-2}$ for W49A. From Mezger et al. (1967), $F_{\nu}(1.41 \text{ GHz}) = 30 \pm 3 \text{ Jy}$.

³ Notable exceptions to this correlation are radio galaxies and radio-loud QSOs, which have q values typically lower by a factor of $\sim 2 - 4$ (see Sanders & Mirabel (1996) and references therein).

These values yield $q = 3.36$, which is significantly higher than the average value found in normal galaxies and starbursts, and even higher than the typical q values obtained for ULIRGs.

Given the high q value derived above for W49A, which is *entirely* dominated by extremely young and embedded massive stars, we might also expect to find a high q value for the galaxies in which we have detected UDHIIs. Using the IRAS Point Source Catalog fluxes, we find that He 2-10 has $\text{FIR} = 1.12 \times 10^{-12} \text{ W m}^{-2}$ and NGC 5253 has $\text{FIR} = 1.39 \times 10^{-12} \text{ W m}^{-2}$. From Kobulnicky & Johnson (1999), $F_\nu(1.42 \text{ GHz}) = 70 \pm 7 \text{ mJy}$ for He 2-10, and from Turner et al. (1998) $F_\nu(1.49 \text{ GHz}) = 76 \pm 2 \text{ mJy}$ for NGC 5253. The resulting q values are 2.63 and 2.69 for He 2-10 and NGC 5253, respectively, and are both significantly higher than the average value derived for starburst galaxies, but consistent with the typical value of ULIRGs. Even after correcting the radio flux from He 2-10 for self-absorption according to the prescription given by Condon et al. (1991b), q is still significantly higher than the canonical value with the corrected value of $q = 2.5$.

The most straightforward interpretation is that bulk of the star formation in He 2-10 is so young that it has not yet begun to produce SNe in the relative numbers typical in most galaxies, in agreement with the result for the embedded clusters in § 4.5.3. In other words, while the five embedded clusters in He 2-10 are largely (or solely) responsible for the mid- to far-infrared flux, they are not yet mature enough to produce synchrotron radiation in amounts necessary to obtain the standard q value.

How does the q value of the nearby starburst M82 (where there currently don't appear to any UDHIIs) compare? From Kuehr et al. (1981), the 1.4 GHz flux of M82 is 8.6 Jy, and from Soifer et al. (1989) values for the 100 μm and 60 μm fluxes are 1355 Jy and 1313 Jy, respectively. I calculate $\text{FIR} = 5.98 \times 10^{-11}$, which results in $q = 2.27$. This q value is in excellent agreement with those derived for other galaxies by Condon et al. (1991b), but significantly lower than the values derived above for He 2-10 and NGC 5253, both of which are known to host UDHIIs, while M82 does not.

Although we have a sample size of only two galaxies hosting UDHIIs, they both have

$q > 2.6$, while the local starburst M82 which does not host UDH IIs have a q value significantly lower. This trend is exactly what we would expect for galaxies undergoing vigorous star formation and hosting massive UDH IIs. This tentative result lends itself two main implications: (1) q values might be useful for identifying galaxies which are most likely to host UDH IIs, and (2) because high q values are typical of ULIRGs, UDH IIs might have a significant role in powering their infrared luminosities.